https://doi.org/10.5194/egusphere-2025-6183
Preprint. Discussion started: 13 January 2026

Improving the representation of coastal polynyas in high resolution climate models with satellite datasets

José Abraham Torres-Alavez[1], Ruth Mottram[1], Thomas Lavergne[2], Rasmus Pedersen[1], and Ole Bøssing Christensen[1]

[1]Danish Meteorological Institute, Copenhagen, Denmark
[2]Norwegian Meteorological Institute, Oslo, Norway

Correspondence: José Abraham Torres-Alavez (jat@dmi.dk)

Abstract. Coastal polynyas are primarily wind driven openings in the sea ice close to shore. They are important drivers of sea ice production, ocean circulation and have important consequences for polar ecology. Accurate understanding and modelling of the Earth system in the polar regions requires a thorough representation of polar climate processes including polynyas and sea ice. This paper investigates the evolution of coastal polynyas and their atmospheric impacts in Greenland and Antarctica by analysing two satellite products alongside simulations from a regional climate model (RCM). We examine how the representation of polynyas differs between the satellite datasets and how these differences affect the RCM when used as boundary conditions. We further explore how the modelled polynyas influence surface atmospheric conditions, boundary layer and cloud properties. Our analysis is based on the Harmonie-Climate (HCLIM) regional climate model, which employs spectral nudging and a surface scheme optimised for polar regions. The model provides a flexible framework for process studies, including with direct use of Earth Observation data such as a new higher spatial resolution satellite product, developed by the ESA climate change initiative (CCI) for sea ice. We run the model over both polar regions, to examine the impact of coastal polynyas in northern Greenland in 2018 and Terra Nova Bay in Antarctica in 2010. Comparison between runs shows an improved representation of climate with the high resolution sea ice product, particularly in boundary layer properties and near the coast which standard resolution sea ice data often has difficulty capturing. Our results show that using the high resolution CCI sea ice data directly in regional climate models can improve characterisation of near-surface weather and climate, supplementing the use of fully coupled atmosphere -ocean- sea ice modelling for process understanding and argue for the inclusion of this data in assimilation systems used for reanalysis.

1 Introduction

Coastal polynyas are a key feature of the polar regions at the interface of atmosphere, ocean, sea ice and biology. Driven by atmospheric processes, namely strong offshore winds, they are often sustained by ocean dynamics and are important drivers of global ocean circulation via the production of Antarctic bottom water, local and regional sea ice production and marine productivity (Golledge et al., 2025). Coastal polynyas are found in both Arctic and Antarctic and have many common features between the two poles, particularly at the surface interface with the atmosphere. Representation of polar climate in numerical

https://doi.org/10.5194/egusphere-2025-6183
Preprint. Discussion started: 13 January 2026

climate models requires the inclusion of all elements of the polar earth system, including the cryosphere and polynyas are an often neglected feature (Golledge et al., 2025) due in part to the high resolution needed to resolve them which is not possible in most global climate models (GCMs). Indeed, traditional GCMs have frequently been criticised for poor representation of sea ice in general, including for failing to model the observed decline in sea ice area in the Arctic over the last 40 years (Stroeve et al., 2012). The consequences for this relatively poor performance, include poor representation of local weather and climate, particularly close to the coast or in ice marginal areas, as well as impacts on clouds, energy and moisture budgets and on ocean properties where sea ice is not well represented (Rinke et al., 2006). As regional climate models (RCMs) are strongly constrained by the driving GCMs, they likewise suffer similar problems in characterising sea ice cover, but their high resolution makes them more suitable than GCMs to resolve polynyas and the processes like high surface wind speeds and ocean-atmosphere heat and moisture fluxes that drive them. However, coupled atmosphere- ocean regional models are complex and computationally expensive to run. They also have a tendency to drift that is unhelpful for comparisons with in situ observations (Sauerland et al., 2025). A intermediate and computationally cheaper solution is therefore to apply a realistic sea ice lower boundary condition into an atmospheric climate model in order to assess surface fluxes and atmospheric feedbacks. In this paper we apply the HARMONIE-Climate (HCLIM) regional climate model (Belušić et al., 2020; Lind et al., 2022) to assess the role of polynyas in affecting local climate. As the model is atmosphere only, we also use a newly developed satellite dataset of high resolution sea ice data from the ESA CCI for sea ice concentration as a new lower boundary data set and compare the output with control simulations driven by the OSI-SAF. Our study therefore seeks to not only test the new set-up of a new generation RCM, but also to assess if inclusion of a new sea ice dataset that resolves polynyas on a finer scale can assist in improving local and regional climate model simulations and understanding the fluxes between atmosphere and ocean.

2 Background

Sea ice is a defining feature of the polar regions, the long-term decline of Arctic sea ice superimposed on the annual cycle of waning and waxing has become a definitive sign of a changing global climate (Kwok and Rothrock, 2009). More recently, after decades of stability, Antarctic sea ice has also showed signs of decline in area. However, global climate models have struggled to model these changes realistically (Notz and Community, 2020; Roach et al., 2020). Coastal polynya occurrence in the Arctic and Antarctic is currently stable in both area and frequency of occurrence, likely because these features are mostly prominent in winter. Coastal polynyas differ from open water polynyas as they are primarily formed in the pack ice close to shore by katabatic winds (Golledge et al., 2025). Strong winds push ice off shore away from the coast, leaving open water which then starts to freeze again, the newly forming ice is then further pushed away again by persistent winds. The formation of sea ice leads to significant brine rejection and the formation of dense water, particularly in the Antarctic (Wei et al., 2021). As this dense shelf water sinks it is likely an important source of Antarctic bottom water and therefore part of the global thermohaline circulation (Golledge et al., 2025). The presence of open water in the pack ice also allows large fluxes of energy and moisture at the atmosphere-ocean surface, affecting local weather and climate and with important consequences for ecology as well as the physical environment (Morales Maqueda et al., 2004; Noel et al., 2025).

https://doi.org/10.5194/egusphere-2025-6183
Preprint. Discussion started: 13 January 2026

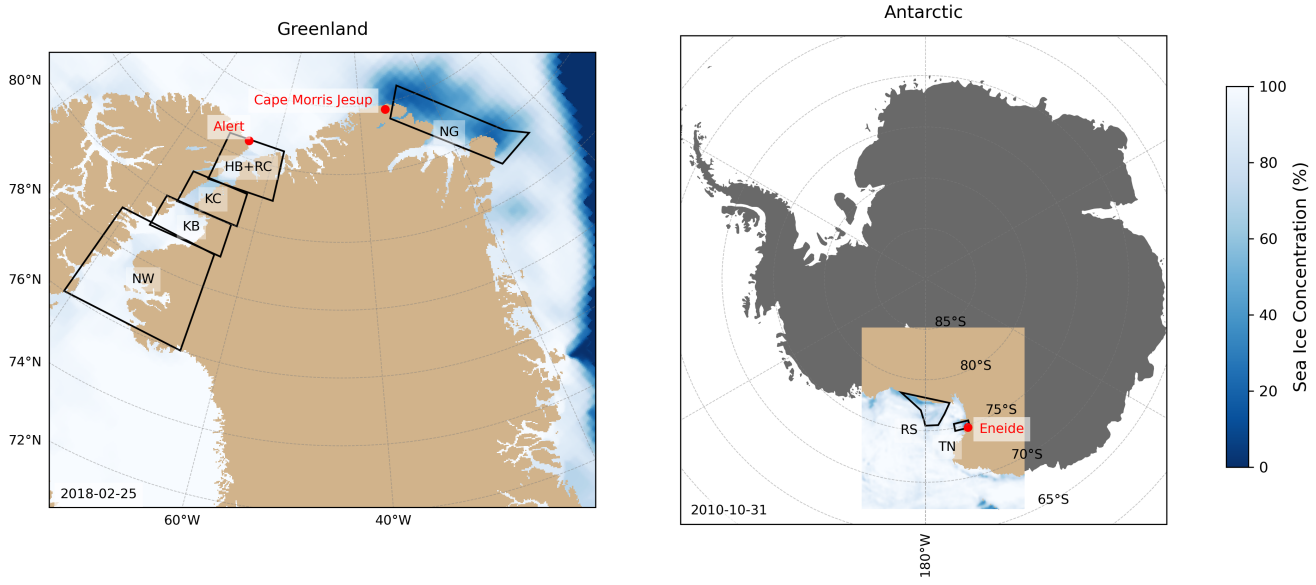

Figure 1. Sea-ice concentration for the Greenland domain (left) and Antarctic Domain (right) used in these experiments. The abbreviations for locations along Nares strait are: North Water (NW); Kane Basin (KB); Kennedy Channel (KC); Hall Basin (HB) and Robeson Channel (RC). The abbreviations for locations in Antarctica are: Ross Sea (RS) and Terra Nova (TN).

Given their importance, we have focused on simulating two polynyas in northern Greenland, the annually reccurring North Water polynya with its ice arches and the rare North Greenland polynya, that formed in 2018, and two regularly occurring polynyas in Antarctica, at Ross Sea and Terra Nova Bay (Fig. 1).

2.1 The North Greenland Polynya

During February-March 2018, an unusual and extensive polynya of approximately 60,000 square kilometers was observed north of Greenland between the Lincoln and Wandell seas (Ludwig et al., 2019). Peaking between the 10th February and 12th march, this notable event occurred when this region is typically covered in thick, multi-year ice. However, in February 2010, a sudden stratospheric warming event, in conjunction with a reversal of the stratospheric winds, produced strong, sustained, warm surface winds, exceeding 25 m/s (Lee et al., 2023). These winds blew from the south, generating temperatures above freezing (Moore et al., 2018) for almost 10 days before the event. The strong offshore winds and warm temperatures pushed the ice away and prevented new ice from forming from mid-February to early March.

2.2 The North Water Polynya

The North Water polynya is an extremely important feature of the local environment in NW Greenland. It provides a large number of marine mammal and fish resources for both commercial fisheries and local subsistence, as well as being a diversity hotspot (Vincent, 2019). The opening of the polynya is driven by wind forcing through the Nares Straits and associated with

https://doi.org/10.5194/egusphere-2025-6183
Preprint. Discussion started: 13 January 2026

the build up of a sea ice arch at the north end (Moore et al., 2023). The narrow topography in this region means that high resolution climate models are particularly important for capturing local scale wind forcing that causes the polynya to form. A long-running research and programme by DMI based in the nearby community of Qaanaaq also allows us to assess the performance of the model and to better understand the processes important for the polynya and it's wider impact on the local environment.

2.3 Terra Nova Bay and Ross Sea Polynyas

The Terra Nova Bay and Ross Sea polynyas regularly forms in Antarctica by the Ross Ice shelf. It is similar to the other two coastal polynyas in that it is driven by strong katabatic winds from the ice sheet. Several studies have also pointed to the importance of the opening of this polynya on seal populations in the region, as the open water allows them to hunt effectively. (Thompson et al., 2020; Fonseca et al., 2023)

2.4 Regional Climate Modelling

Regional climate models (RCMs) give high quality climate information at high resolution (tens of km to sub-km horizontal resolution) over a limited area of the world. As such they are often used for providing climate services such as assisting efforts to plan for and adapt to climate change and there high horizontal resolution makes them ideal for representing smaller scale features like polynyas. In the polar regions, RCMs have long been used to provide information on the cryosphere including for example, ice sheet surface mass balance (Fettweis et al., 2020; Mottram et al., 2021), permafrost processes and the impact of sea ice changes on regional climate. RCMs are commonly used to provide climate simulations at the present day but also for dynamical downscaling of global climate simulations to provide climate projections at higher resolutions. The WCRP (World Climate Research Programme) Co-Ordinated Regional Downscaling EXperiment (CORDEX) provides a set of guidelines for RCM groups to follow to allow for an easier and standardized model intercomparison (Koenigk et al., 2015), which we mostly follow in this study (see Methods section below). At the lower boundary of most RCMs the sea ice and sea surface temperature is simply imported and interpolated to the grid from the driving model, usually climate reanalysis for present day simulations or a global climate model forcing for future projections. This means that RCMs inherit some of the bosses of coarser resolution models and don't resolve smaller scale features. Coupled RCMs which use sea ice and ocean models are in development but they are expensive to run and often suffer from initialisation problems and drift with different model components not being in phase with each other or with the observed climate as represented in a reanalysis which makes it complex to compare outputs with in situ observations (Sauerland et al., 2025). The assimilation of sea ice data directly into regional climate models is rather uncommon, though it is more often used in reanalysis including regional reanalysis (Schyberg et al., 2020; Batrak et al., 2024). However, global models and particularly those run as seasonal and decadal prediction systems have developed and do run assimilation systems as part of efforts to both understand the drivers of sea ice variability on a seasonal scale and to understand the effects on the regional and global climate system of sea ice variability (Blanchard-Wrigglesworth et al., 2011; Tietsche et al., 2013; Day et al., 2014). In this study we experiment with high resolution (4 - 2.5 km) RCM simulations as well as a new

https://doi.org/10.5194/egusphere-2025-6183
Preprint. Discussion started: 13 January 2026

high resolution (12km) satellite dataset of sea ice to assess if the representation of coastal polynyas in climate models can be improved, paving the way for future process studies.

3 Methods

3.1 Regional Climate Model HCLIM

The RCM HCLIM is built on the numerical weather prediction (NWP) model developed by the HIRLAM-ALADIN consortium (Bengtsson et al., 2017). As described by Belušić et al. (2020) the model can be run at scales ranging from kilometre scale and convection-permitting to mesoscale (tens of kilometres. In this study we take advantage of the AROME physical schemes to run at a high resolution of 4km and 2.5km for Greenland and Terra Nova Antarctica, respectively; with 65 vertical levels and time step of 45 second in both simulations. This horizontal resolution is chosen to better represent the evolution of the polynyas. The HCLIM-AROME model is described in detail in Belušić et al. (2020) and Lind et al. (2022), but we have also implemented some changes. Notably, we implemented and tested a spectral nudging scheme (Berg et al., 2013; Mottram and Consortium). Spectral nudging is a form of assimilation within the domain that prevents the modelled weather drifting too far from the boundary forcing by also applying some forcing within the model domain (Von Storch et al., 2000).

HCLIM-AROME is a non-hydrostatic model with a semi-Lagrangian advection scheme and a semi-implicit time discretisation. Although the deep convection is no longer parameterised, the sub-grid shallow convection is still parameterised, using the EDMFm scheme based on the eddy diffusivity mass-flux framework (Bengtsson et al., 2017; Rooy and Siebesma, 2008). The parameterization of the turbulence use the prognostic equation for the turbulent kinetic energy (TKE) combined with a diagnostic length scale (Lenderink and Holtslag, 2004; Bengtsson et al., 2017).

HCLIM contains the sea ice module SICE (simple ice scheme) which represent the temperature profile using a thermodynamic approach (Batrak et al., 2018).

A spectral nudging technique (Von Storch et al., 2000; Radu et al., 2008) is applied to HCLIM-AROME in order to impose large-scale conditions. It was applied to vorticity with an e-folding time of 6 hours, for air temperature at 24 hours and divergence at 48h. We do not nudge surface pressure or humidity.

Spectral nudging is applied only to the long waves, whose physical wavelength is greater than 800 km, and has been applied just above the planetary boundary layer (PBL) to allow the small-scale processes near the surface to be free to respond to local processes (Lo et al., 2008). For our simulations, the spectral nudging starts at 850 hPa and increases exponentially until it reaches 100% at 700 hPa and remains until the top of the atmosphere.

We conducted a series of sensitivity experiments. They deal with the dependency of the simulation to different sea-ice boundary conditions. The dependency on different boundary conditions is examined by considering a series of HCLIM-AROME simulations that differ very little among each other. It consists of two runs for northern Greenland, for February-March 2018, and two over Terra Nova, Antarctica for October-November 2010. The lateral boundary-forcing (BC) data in each event are provided by the 3-hourly ERA5 data with exception of the sea ice concentration (SIC) lower boundary forcing data, which are updated daily and represent the only BC difference between the runs. For each domain, simulations are performed using SIC

https://doi.org/10.5194/egusphere-2025-6183
Preprint. Discussion started: 13 January 2026

lower boundary forcing data sets from (1) CCI+SIC at 12.5-km resolution, and (2) OSI SAF SIC dataset at 25-km resolution. In our simulations, the sea surface temperature in ice free grid cells is not modified directly by the input of satellite observed SSTs, but is derived from the ocean boundary condition. If the grid cell has sea ice (from the satellite datasets), the ice surface temperature is calculated using the SICE model. This model adjusts the heat diffusion equation and the momentum flux drag according to the presence or absence of sea ice.

Figure 1 shows the sea-ice concentration from OSI-SAF for a day of maximum extension of the polynyas for both domains simulated using HCLIM and identified in data from the weather stations used in this study. The atmospheric fields analyzed are not corrected because the stations are not higher than 100 m above sea level (Table 1), and the correction would not be significant.

3.2 Sea Ice Concentration data

The two sea-ice concentration (SIC) datasets used in this study are the SIC Climate Data Record (CDR) version 3 from the EUMETSAT Ocean and Sea Ice Satellite Application Facility (OSI SAF) OSI-450-a (OSI SAF and EUMETSAT SAF On Ocean And Sea Ice, 2022), and the High(er) resolution SIC CDR from the ESA Climate Change Initiative (CCI) SICCI-HR-SIC (Lavergne et al., 2023a).

Both CDRs are multi-decadal datasets derived from raw brightness temperature measurements recorded by space-borne passive microwave radiometers, specifically on board the Special Sensor Microwave/Imager (SSM/I) and Special Sensor Microwave Imager-Sounder (SSMIS) satellite series. The two datasets are tightly related: SICCI-HR-SIC is an enhanced-resolution version of OSI-450-a. Lavergne et al. (2019) provides an in-depth introduction to the algorithms used to prepare (previous versions of) the SIC CDRs, while Lavergne et al. (2023b) briefly covers the new developments specific to OSI-450-a and SICCI-HR-SIC, in particular the methodology to enhance spatial resolution using the high frequency and high(er) resolution imagery of the SSM/I and SSMIS instruments.

OSI-450-a covers the period 1978 - 2020 and is extended by an Interim CDR (ICDR) from 2021 onwards. SICCI-HR-SIC covers the period 1991 - 2020. At time of writing, it is not extended with an ICDR. It starts in 1991 with the first SSM/I satellite with functioning high frequency imagery.

OSI-450-a is prepared on Equal Area Scalable Earth (EASE2) grids with 25 km spacing, but the true resolution of the data is coarser, probably 30-50 km owing to the footprint size of the imagery channels entering the algorithm. SICCI-HR-SIC is prepared on the same EASE2 grids, but with a 12.5 km spacing.

As part of this study, the two SIC CDRs are remapped and resampled to the high-resolution grids of the HCLIM runs. This involves filling coastal HCLIM grid cells from neighbouring (off-shore) SICs.

Being based on relatively coarse satellite observations, the two SIC CDRs are not free from errors and uncertainties. Of particular relevance here, these CDRs (and other similar datasets based on the same satellite measurements) are known to 1) overestimate SIC in the coastal regions due to land spill-over contamination of the satellite signal, 2) general underestimation of thin (<20 cm) sea ice, 3) increased uncertainties and biases during the summer season in the presence of wet snow and melt

https://doi.org/10.5194/egusphere-2025-6183
Preprint. Discussion started: 13 January 2026

ponds. For a detailed investigation of the qualities and weaknesses of SIC CDRs, refer to Lavergne et al. (2019); Kern et al. (2019, 2020, 2022) and the dataset documentation.

3.3 CARRA reanalysis

To evaluate the Arctic simulations, we use the CARRA Copernicus Arctic Regional Reanalysis (Schyberg et al., 2020). The CARRA dataset is freely available on the Copernicus climate data store and covers two domains including one covering the whole of Greenland that is close to the set up used by HCLIM. CARRA is run as a regional reanalysis on the boundaries by ERA-5 but has a great deal of additional observational data assimilated into it, much of which is not included in ERA-5, making it the best representation of many surface and atmospheric processes in the region. Although it is also based on the AROME model, CARRA is run with a different, more recent model version (Cycle 40), at 2.5 km horizontal resolution, and also includes data assimilation of high-resolution ocean surface data, however sea-ice concentration in CARRA is derived from the OSI-450 and SICCI products at 25 km resolution. Our study is this also an opportunity to assess if the higher resolution sea ice dataset can give improvements in other reanalysis type simulations.

3.4 Evaluation with automatic weather stations

Coastal polynyas usually occur in under-resourced regions with scarce observational data in situ. We are therefore forced to use automatic weather stations (AWS) that are as close to the polynyas as possible but which are still maybe tens or hundreds of km distance.

4 Results

Figure 2 shows the evolution of the polynya over Greenland for the two products used as sea-ice boundary conditions, OSI SAF (left column) and ESA CCI (middle column), as well as the difference between them (right column). For February 10, 2018, a minimum of sea-ice concentration appeared in the northeastern part of Greenland in both datasets. Other sea-ice concentration minima occurred over the Kennedy and Robeson channels in western Greenland, both of which are more intense for ESA-CCI. This polynya in the Narest Strait was observed through the study period, with a different extent but lower sea-ice values in ESA-CCI than in OSI SAF. Both satellite products showed a difference in the location of the marginal ice zone in the eastern part of the domain during the study period. For February 15, 2018, both datasets showed an increase in sea-ice concentration over the whole domain, with a larger increase for OSI-SAF than ESA-CCI in the northeastern part of Greenland, while for the Narest Strait, the increase is larger for ESA-CCI. On February 20, 2018, the polynya began to form over the northeastern coast of Greenland from Cape Morris Jesup to the northern part of the Greenland Sea, with OSI-SAF showing 20% more ice than off the coast of Peary Land. However, ESA-CCI showed more sea ice in the fjords of this area. On February 25, the polynya reached its maximum extent from Cape Morris Jesup to the Greenland Sea, with ESA CCI showing less ice than OSI SAF over the Wadel Sea, but the opposite over the fjords. For March 2, 2018, the polynya disappeared, with an increase in sea-ice concentration of up to 50%, but ESA CCI still showed lower sea-ice values than OSI SAF. The polynya was completely closed

https://doi.org/10.5194/egusphere-2025-6183
Preprint. Discussion started: 13 January 2026

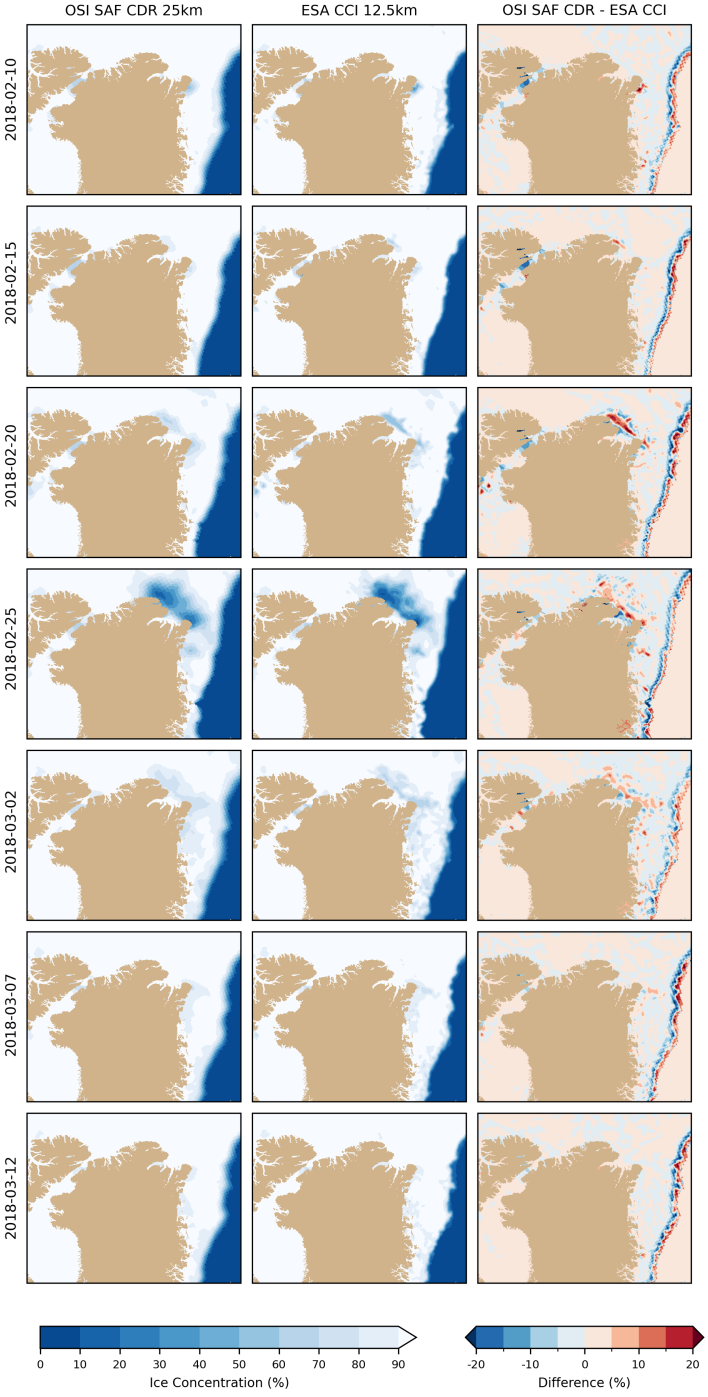

Figure 2. Evolution of polynyas in northern Greenland from 10 February to 12 March 2018; for OSI SAF (left column), ESA CCI (middle column) and the difference between them (right column).

https://doi.org/10.5194/egusphere-2025-6183
Preprint. Discussion started: 13 January 2026

in the Wadel Sea on March 7, while sea ice was still recovering over the Greenland Sea, with similar values of 80% in both datasets. On March 12, both products showed similar high sea-ice cover over the region.

We examined the sea-ice area in the North Water Polynya, along Nares Strait, and in the North Greenland Polynya (Fig. 3). The hourly time series reveal distinct regional differences in the timing of the annual minimum. In the North Water Polynya, the minimum area occurred on 23 February, followed one day later in Kane Basin. For Kennedy Channel, the two satellite datasets diverged, OSI SAF indicated the minimum on 24 February, while ESA CCI placed it on 27 February. In Hall Basin and Robeson Channel, the minimum occurred on 28 February, and over the North Greenland Polynya on 26 February.

Overall, the two satellite products do not show systematic spatial or temporal differences beyond features resulting from the different resolution. Over the North Water Polynya, ESA CCI reported a larger sea-ice area than OSI SAF until 25th February, after which the differences dropped below 2000 km^2. In Kane Basin, the differences were generally smaller than 1000 km^2, but OSI SAF consistently showed higher sea-ice values. Over Kennedy Channel, a shift occurred on 25 February: before this date, ESA CCI estimated more ice, but afterward OSI SAF showed larger values, with an average difference of about 4000 km^2 through 3 March. In Hall Basin and Robeson Channel, OSI SAF consistently showed higher sea-ice values, while over the North Greenland Polynya ESA CCI reported lower values, by as much as 8000 km^2.

Because open water strongly enhances evaporation, we tracked how these sea-ice differences influenced the latent heat flux (Fig. 3). The representation of polynyas in the two products clearly affected surface fluxes: latent heat fluxes peaked when sea ice reached its minimum, increasing by almost a factor of five across all regions. For the North Water Polynya, Kane Basin, and the North Greenland Polynya, the differences between ESA CCI and OSI SAF remained below 5 W/m^2. However, in Kennedy Channel, Hall Basin, and Robeson Channel, differences reached up to 40 W/m^2 during 22–28 February. Compared with CARRA, our simulations generally have higher latent heat fluxes, with the largest differences coinciding with periods of minimum sea ice.

The moisture released from polynyas also contributes to cloud formation. To examine this effect, we analyzed low-level cloud cover (Fig. 4). Consistent with the small differences in latent heat flux, cloud cover over the North Water Polynya, Kane Basin, and the North Greenland Polynya showed almost identical temporal evolution between the two products. Over Kennedy Channel, however, differences in low-level cloud cover reached 20% between 25–27 February. In Hall Basin and Robeson Channel, ESA CCI indicated higher low-level cloud fractions than OSI SAF, despite OSI SAF showing higher latent heat fluxes. This mismatch suggests that in this area, moisture transport from the south may play a dominant role in cloud formation. Compared with CARRA, the HCLIM model captures the temporal variability of cloud cover over the Greenland polynyas, but it tends to underestimate cloud cover during certain periods.

The increase in cloud cover associated with enhanced latent heat flux from the polynyas also influences the surface radiation balance (Fig. 4). In particular, higher fractions of low-level cloud coincided with stronger downwelling longwave radiation. On 26–27 February, the differences in downwelling longwave radiation between HCLIM–ESA CCI and HCLIM–OSI SAF were largest, ranging from 5 to 22 Wm^{-2}, with the maximum values over Kennedy Channel. For the remainder of the period, however, the differences between the two simulations were minimal. During this period, shortwave radiation plays a negligible role because the region remain sunless during late winter.

https://doi.org/10.5194/egusphere-2025-6183
Preprint. Discussion started: 13 January 2026

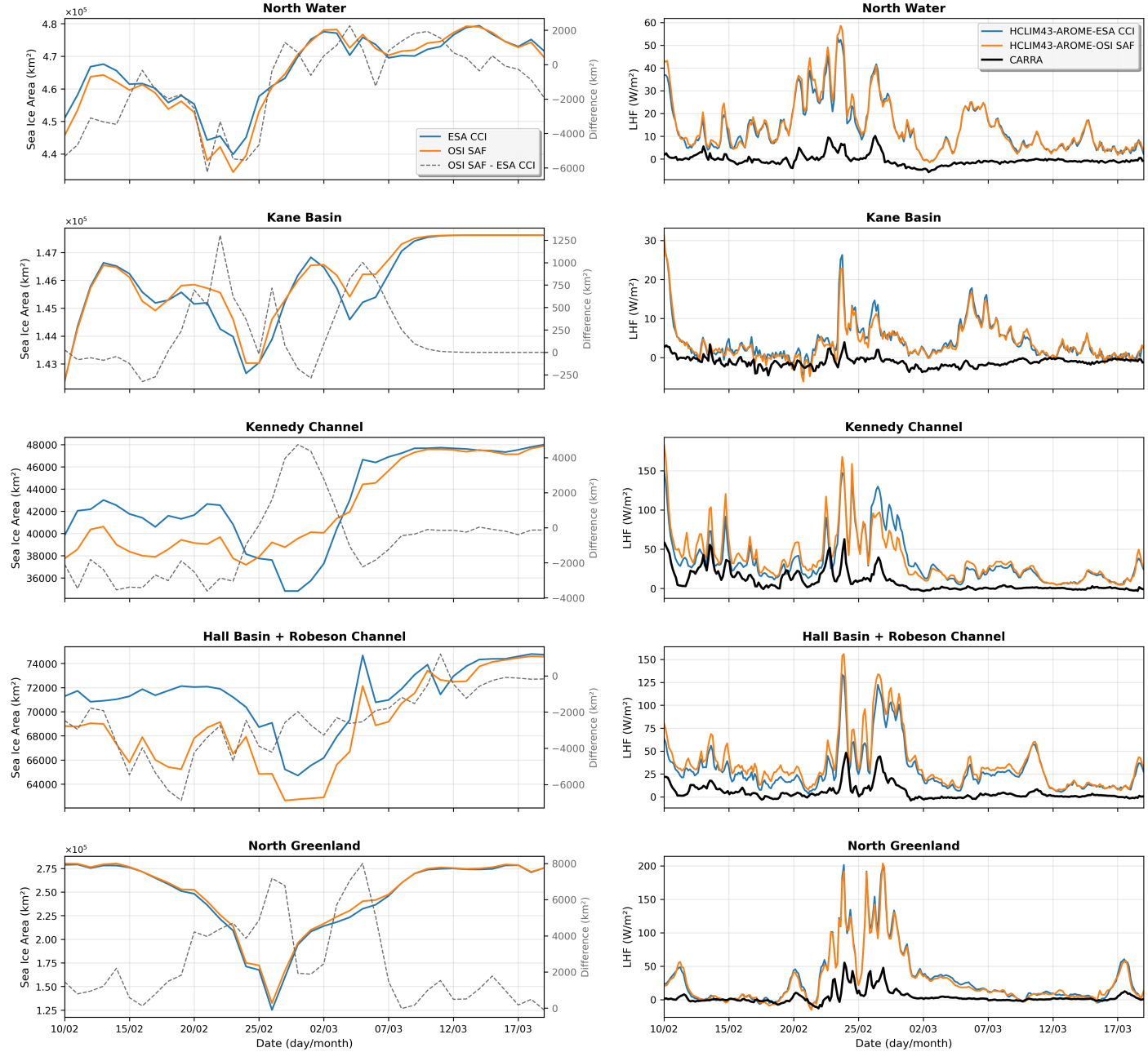

Figure 3. Left panel: Sea-ice area (km^2) from ESA CCI and OSI SAF products over the Greenland polynyas, together with their differences. Right panel: Latent heat flux (W/m^2) from HCLIM simulations forced with ESA CCI and OSI SAF sea-ice concentrations, compared with CARRA reanalysis. From top to bottom, the panels correspond to the North Water, Kane Basin, Kennedy Channel, Hall Basin–Robeson Channel, and North Greenland polynyas.

https://doi.org/10.5194/egusphere-2025-6183
Preprint. Discussion started: 13 January 2026

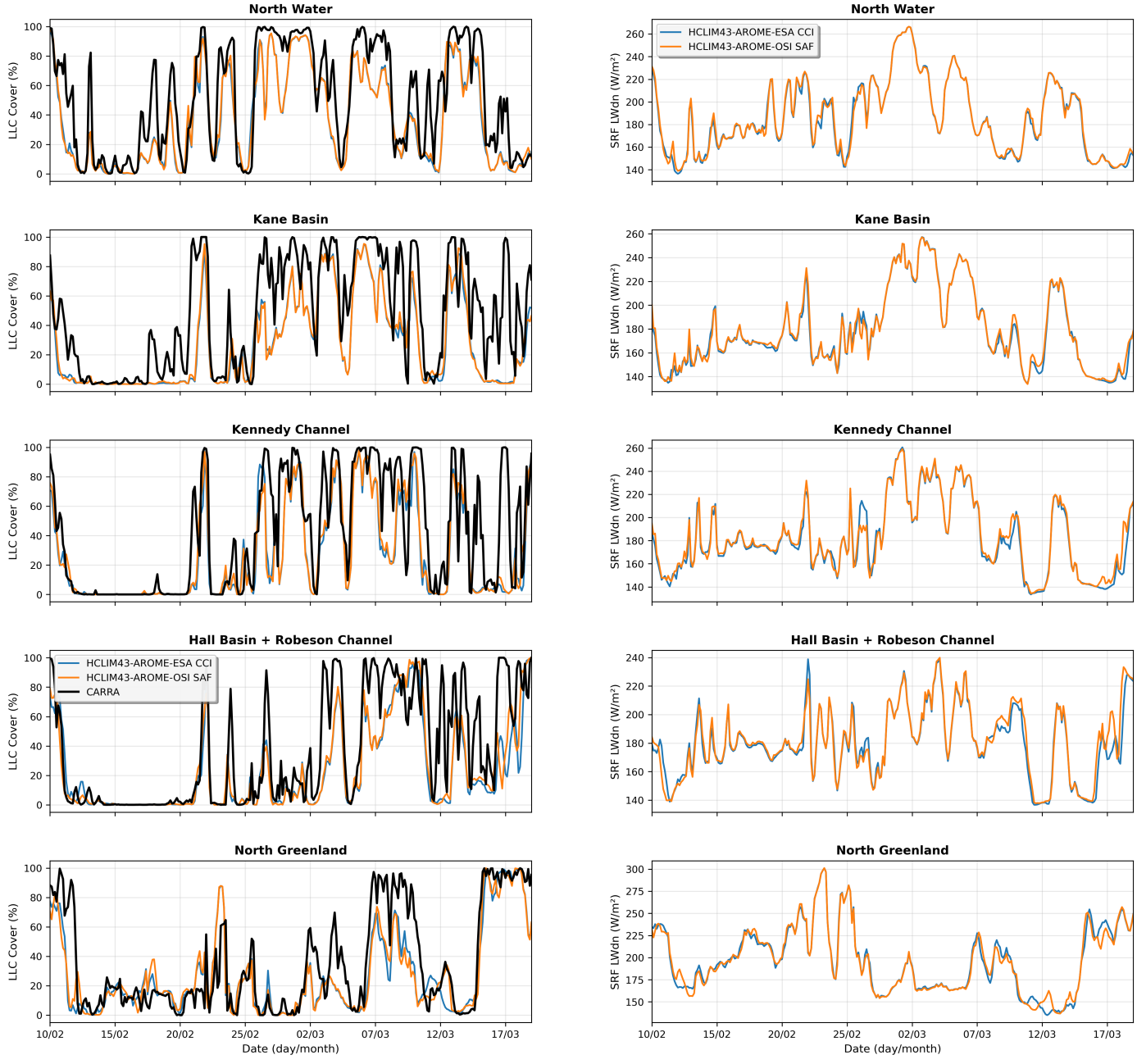

Figure 4. Left panel: Low-level cloud cover (%) from HCLIM simulations forced with ESA CCI and OSI SAF sea-ice concentrations, compared with CARRA reanalysis. Right panel: Downwelling longwave radiation at the surface (W/m^2) from the same simulations and reanalysis. From top to bottom, the panels correspond to the North Water, Kane Basin, Kennedy Channel, Hall Basin–Robeson Channel, and North Greenland polynyas.

https://doi.org/10.5194/egusphere-2025-6183
Preprint. Discussion started: 13 January 2026

The increase in downwelling longwave radiation associated with enhanced low-level cloud cover led to warmer surface conditions. Comparing 2 m air temperatures over the polynyas from CARRA, HCLIM–ESA CCI, and HCLIM–OSI SAF (Fig. 5), we found that the simulations showed only small differences between 14 February and 3 March. After this period, however, the models differ by more than 7 °C, particularly over the Nares Strait polynyas. For the North Water, Kane Basin, and North Greenland polynyas, the differences between the two simulations were negligible, resulting in nearly identical differences compared to CARRA. In Kennedy Channel, the relative performance varied, at times HCLIM–ESA CCI showed smaller differences, while at other times HCLIM–OSI SAF was closer to CARRA. By contrast, over Hall Basin and Robeson Channel, HCLIM–ESA CCI consistently produced smaller differences to CARRA than HCLIM–OSI SAF throughout the period.

From the Hall Basin and Robeson Channel results, we estimate that differences in the sea-ice concentration boundary conditions alone during polynya events can affect surface air temperature by at least 0.5 °C.

The enhanced latent heat flux from the polynyas promotes both cloud formation and, under favourable conditions, precipitation. Figure 5 shows the three-hourly precipitation from the simulations compared with CARRA. Over Nares Strait, five precipitation events were identified during the study period, occurring on 22, 26, and 28 February, and 4 and 6 March. In contrast, in the northern regions of Greenland (North Greenland Polynya, Hall Basin, and Robeson Channel), precipitation was almost absent. Overall, the simulations reproduced the timing of the CARRA precipitation events reasonably well, though they overestimated the intensity of the 28 February and 6 March events in the North Water and Kennedy Channel polynyas. Over Kennedy Channel, precipitation values based on ESA CCI sea-ice concentration were generally closer to CARRA than those from OSI SAF. This result highlights the role that high-resolution sea-ice concentration boundary conditions plays in resolving precipitation in regional simulations.

These results show that the use of high-resolution sea ice concentration data has a stronger impact in improving representation of small polynyas and in regions with complex coastlines, such as the Kennedy Channel, the Hall Basin and the Robeson Channel. It is less important in large polynyas, such as the North Water Polynya and the North Greenland Polynya that are already well resolved in existing satellite datasets.

In order to analyze the effect of the polynyas in the atmospheric fields, both simulations were compared with the observations of Cape Morris Jesup (Figure 6). The observations showed an increase in the temperature of more of 30°C, from February 8 to 20, reaching values above zero on February 20th and 24th, associated with southerly winds. During this period the pressure remained below 1020 hPa, and the relative humidity reached a minimum of 42%. After February 24th, during the maximum extension of the polynya, the air temperature in the models and observations decreased and the pressure and relative humidity increased up to 1040 hPa and 80%, respectively. The simulations are able to reproduce the time series of changes in all the fields with a consistently slightly negative bias for surface pressure up to 10 hPa. For the lowest observed temperatures, the models had a warm bias of up to 10°C, possibly related to inadequately resolved boundary layer processes in the 4km resolution model. For above-zero temperatures, the bias was much smaller in both simulations around -1°C. During the rest of the period, the warm bias was around 5°C. For the relative humidity overall, the bias was positive and less than 10%. Comparing both HCLIM experiments for all the variables, they were almost identical before the maximum extension of the polynya; just after

https://doi.org/10.5194/egusphere-2025-6183
Preprint. Discussion started: 13 January 2026

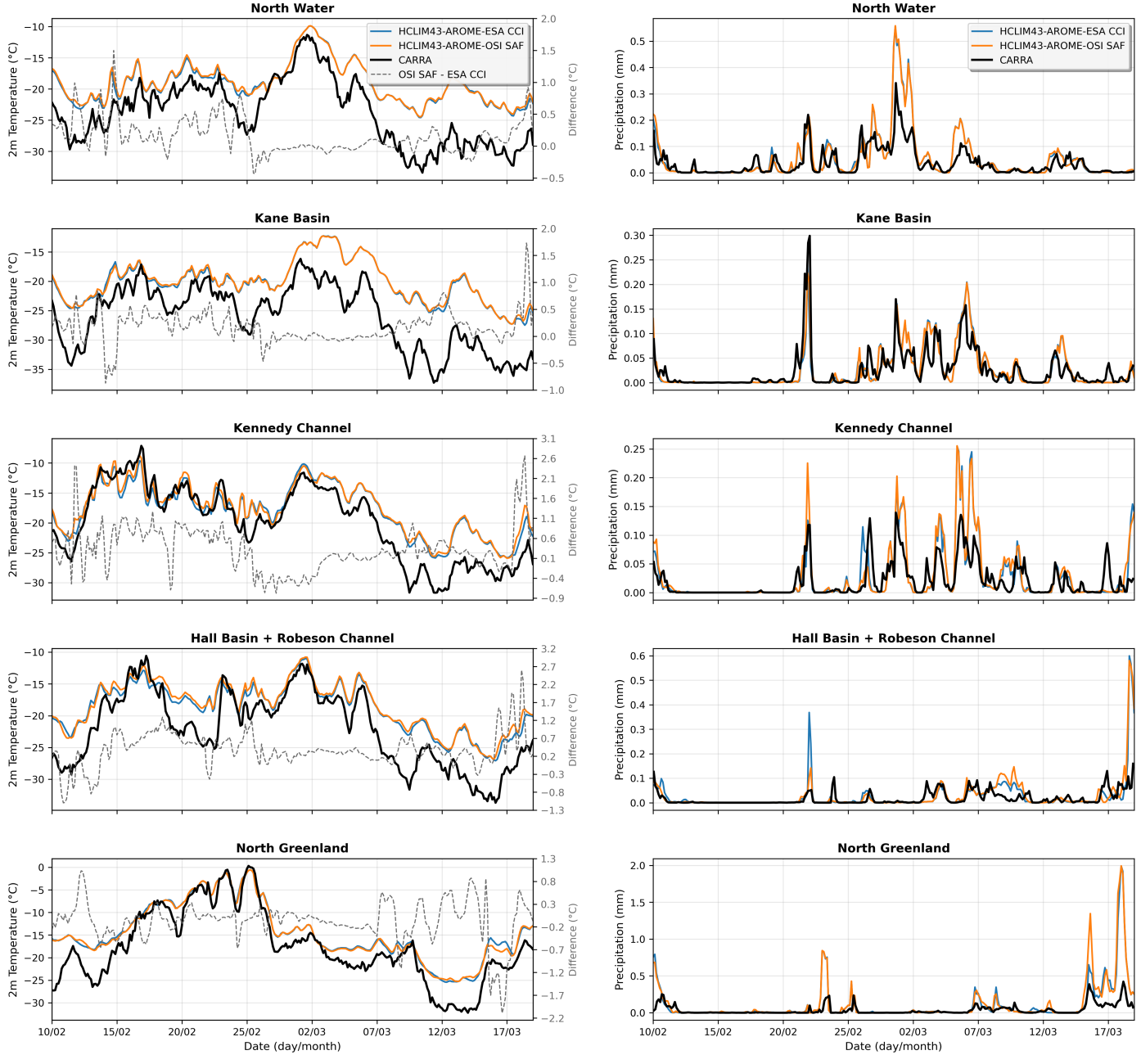

Figure 5. Left panel: 2 m air temperature (°C) from HCLIM simulations forced with ESA CCI and OSI SAF sea-ice concentrations, compared with CARRA reanalysis. Right panel: Precipitation (mm) from the same simulations and reanalysis. From top to bottom, the panels correspond to the North Water, Kane Basin, Kennedy Channel, Hall Basin–Robeson Channel, and North Greenland polynyas.

https://doi.org/10.5194/egusphere-2025-6183
Preprint. Discussion started: 13 January 2026

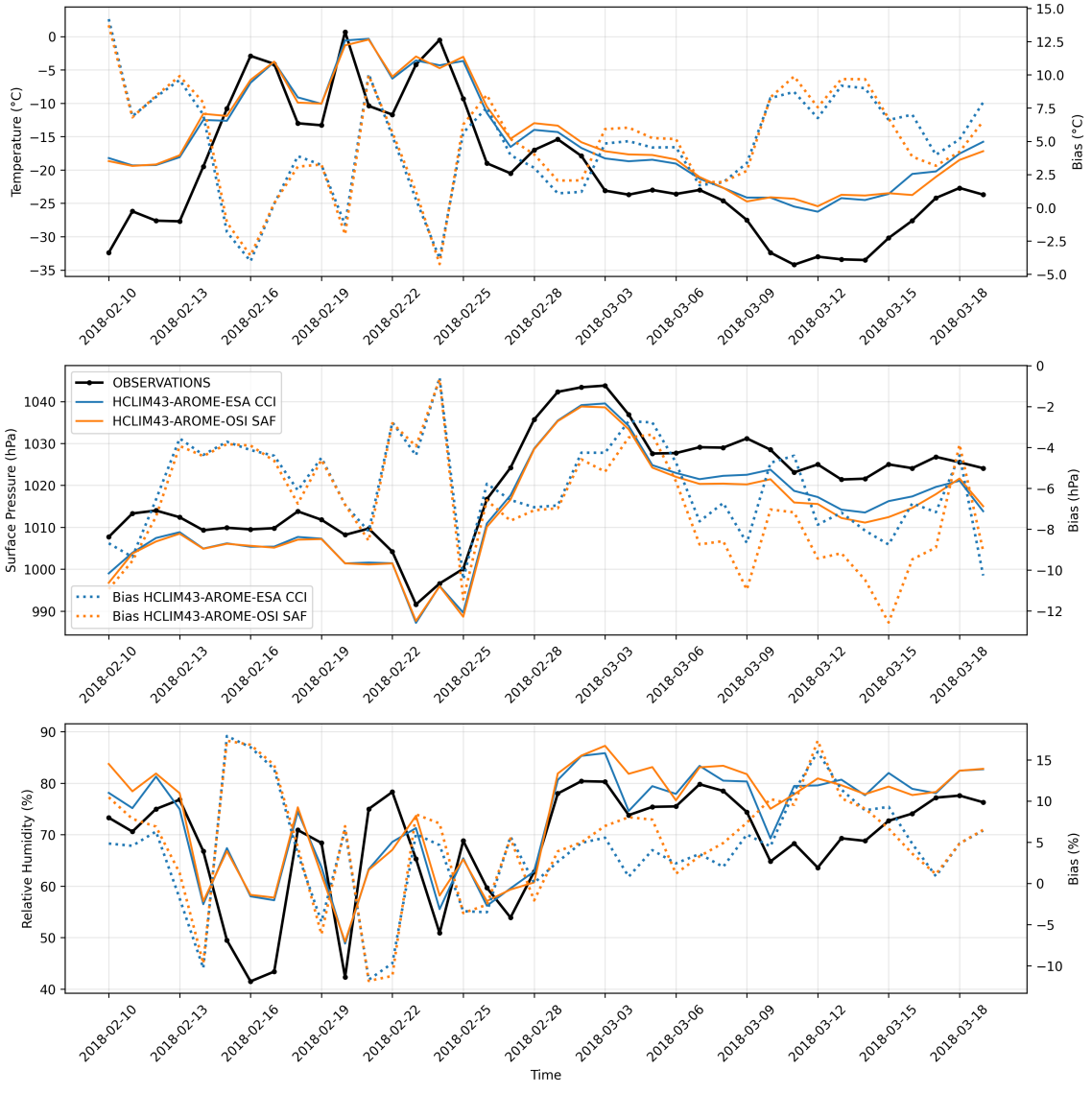

Figure 6. Comparison of observed 2m temperature, surface pressure and surface relative humidity with HCLIM-AROME for Cape Morris Jesup

this, the HCLIM ESA-CCI showed a smaller bias than HCLIM OSI, decreasing by 1°C in temperature, 2hPa in pressure and nearly 10% in relative humidity.

An additional station close to the Kennedy Channel and Hall Basin was also analysed. This is the Alert, Canada, station at Cape Sheridan (Fig. 7). The evolution of the temperature at this station during the simulation showed an increase of 18°C from 8 to 16 February to temperatures above -20°C up to 5th March, after which the temperature started to decrease. The HCLIM

https://doi.org/10.5194/egusphere-2025-6183
Preprint. Discussion started: 13 January 2026

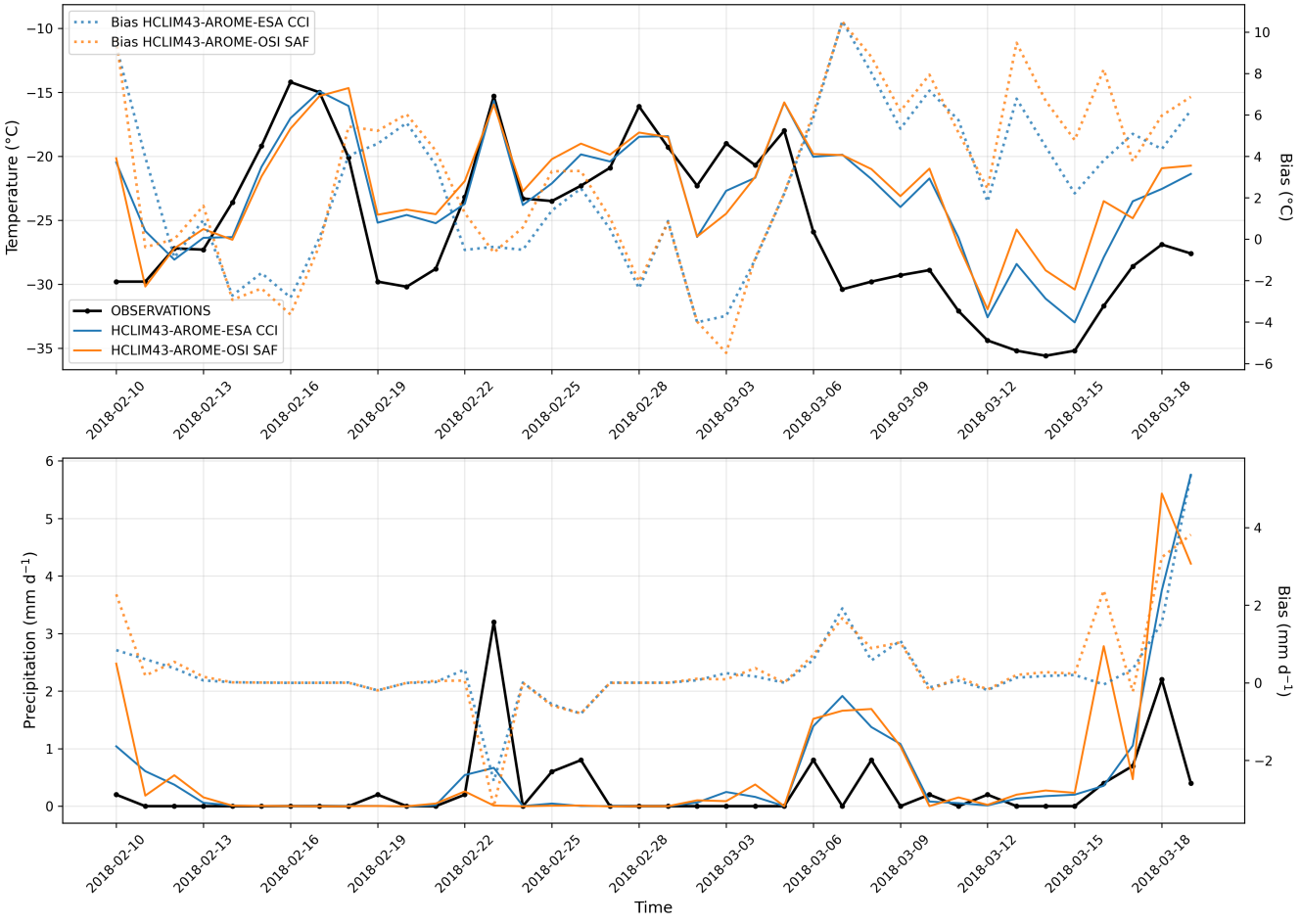

Figure 7. Comparison of observed precipitation and 2m temperature with HCLIM-AROME for Alert, Canada

simulations reproduced the behavior of the temperature time series though with a warm bias reaching 5 °C on 20 February and 12 to 16 March. However, the HCLIM ESA CCI showed a smaller bias than HCLIM-OSI, especially after 24 February, when the HCLIM-ESA-CCI showed a bias smaller than the HCLIM-OSI by 1°C. The Alert station also measured precipitation during the simulated period. The observations showed precipitation of more than 3 mmd^{-1} on 23 February and two events of almost 1 mmd^{-1} on 6 and 8 March. Neither model captures the magnitude of these events. For the first precipitation event, the HCLIM-OSI simulation showed the event one day before, with values of only 0.2 mmd^{-1}; on the other hand, the HCLIM ESA-CCI captured the event on the same day as the observation, but with values of 0.7 mmd^{-1}. For the March events, both HCLIM simulations overestimated the precipitation values by up to 1 mmd^{-1}.

Figure 8 shows the evolution of the polynya over Terra Nova, Antarctica, for the two products used as sea-ice boundary conditions, OSI-SAF (left column) and ESA-CCI (middle column), as well as the difference between them (right column). For October 16, 2010, 70% of the sea-ice concentration appeared at the south end of the Drygalski Ice Tongue in both datasets.

https://doi.org/10.5194/egusphere-2025-6183
Preprint. Discussion started: 13 January 2026

Other sea-ice concentration minima (up to 60%) occurred over the Ross polynya. Between Scott Coast and Ross Island, all showed lower sea-ice values for ESA-CCI. The Ross polynya was observed through the study period and had a different extent. For October 21, 2010, both datasets showed a similar sea-ice concentration: five days for the whole domain. On October 26, 2010, the Terra Nova polynya began to form over the south coast of the Drygalsski Ice Tongue, with OSI-SAF showing sea ice of 80%, 20% higher than those in ESA-CCI, while the Ross polynya showed an extension over previous days. On October 31, the Terra Nova polynya reached its maximum extent, with ESA-CCI showing less ice than OSI-SAF. Something similar occured in the Ross polynya, which increased its extension along of the coast, with less sea ice for ESA-CCI. However, OSI-SAF showed a greater area for this polynya than the higher resolution ESA-CCI dataset. For November 5, 2010, the Terra Nova polynya was less intense than five days before; on the other hand, the Ross polynya showed a reduction in sea-ice concentration and a larger extension to Franklin Island. ESA-CCI still showed lower sea-ice values than OSI-SAF along the coast of the Ross Ice Shelf. The Terra Nova polynya was not completely closed on November 10, though the minimum values of sea ice were limited to the coast, and the Ross polynya was recovering sea ice, particularly over the coast, with similar values of 50% in both datasets. On November 15, both products showed a small Terra Nova polynya more extended in ESA-CCI than in OSI-SAF, while the Ross polynya showed a 30% reduction of sea-ice cover, compared to five days before. Also, gaps of sea ice were found over the Pennell Coast and the region between Ross Island and Scott Coast; on these areas, ESA-CCI showed a higher concentration of sea ice than OSI-SAF close to the shore.

Similar to our analysis of the Greenland polynyas, we examined multiple variables over the Antarctic polynyas. In the period between 5th October and 19th November, the Ross Sea Polynya reached its minimum sea-ice extent on 7 and 16 November, while the Terra Nova Bay Polynya reached its minimum on 8th and 15th November. By comparing sea-ice areas in the HCLIM simulations forced with OSI SAF and ESA CCI, we found that ESA CCI consistently represented smaller polynya extents than OSI SAF in both regions, particularly during 1st–9th November. During this period, the differences in sea-ice area reached approximately 2.9 million km^2 over the Ross Sea Polynya and 0.72 million km^2 over the Terra Nova Bay Polynya (Fig 9).

These discrepancies in polynya extent directly influenced surface–atmosphere exchange. In the Ross Sea, the timing of maximum sea-ice reduction in ESA CCI coincided with a pronounced increase in latent heat flux (Fig. 9), exceeding 75 W m^{-2} between 2nd–9th November. In contrast, over Terra Nova Bay, the model showed a decrease of about 40 W m^{-2} in comparison to previous days. Differences in sea-ice area between the two simulations were also reflected in the latent heat flux, during periods of minimum sea ice, HCLIM–ESA CCI values were roughly 20 W m^{-2} higher than HCLIM–OSI SAF, highlighting the sensitivity of surface fluxes to the choice of sea-ice boundary conditions and the importance of polynyas in the polar climate system.

Enhanced fluxes from the exposed ocean surface supplied additional moisture to the atmosphere, promoting low-level cloud formation. A comparison of the two simulations shows that HCLIM–ESA CCI generally produced more low-level cloud cover than HCLIM–OSI SAF (Fig. 10). Over the Ross Sea, the differences were small (about 1–2%), whereas over Terra Nova Bay they reached up to 14%, with the largest discrepancies occurring between 30 October and 6 November.

These cloud differences also modified the surface radiation budget. Periods of reduced ice and higher cloud cover in ESA CCI were accompanied by enhanced downwelling longwave radiation, particularly over the Terra Nova Bay Polynya, where

https://doi.org/10.5194/egusphere-2025-6183
Preprint. Discussion started: 13 January 2026

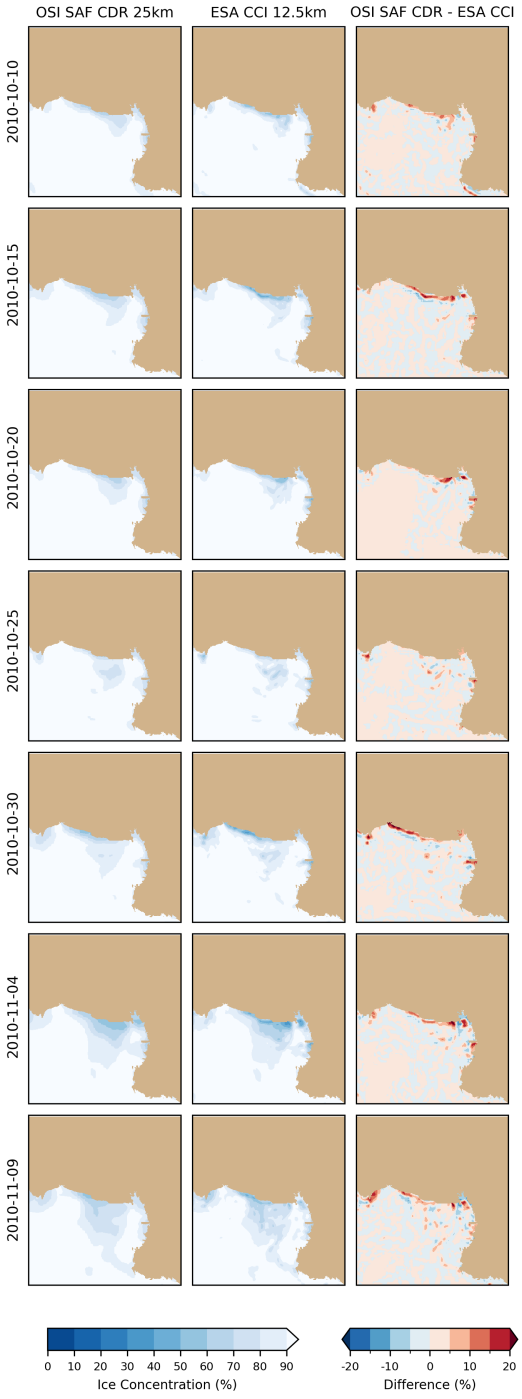

Figure 8. Evolution of polynyas in the Ross Sea, Antarctica from 10 October to 09 November 2010; for OSI SAF (left column), ESA CCI (middle column) and the difference between them (right column).

https://doi.org/10.5194/egusphere-2025-6183
Preprint. Discussion started: 13 January 2026

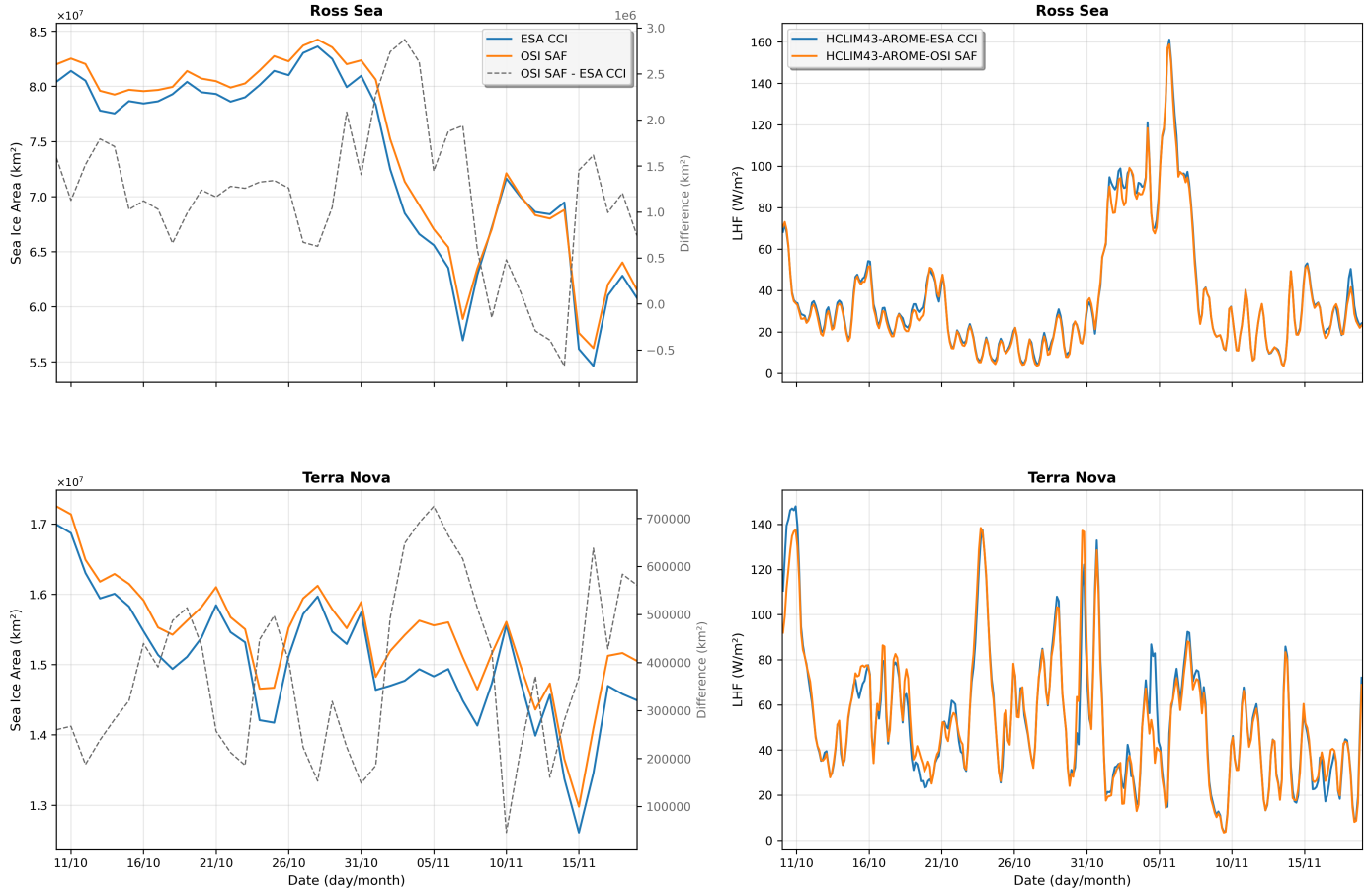

Figure 9. Left panel: Sea-ice area (km^2) from ESA CCI and OSI SAF products over the Antarctic polynyas, together with their differences. Right panel: Latent heat flux (W/m^2) from HCLIM simulations forced with ESA CCI and OSI SAF sea-ice concentrations, compared with CARRA reanalysis. From top to bottom, the panels correspond to the Ross Sea and Terra Nova Bay polynyas.

values were up to 10 W m^{-2} higher than in OSI SAF. The additional longwave input contributed to warmer near-surface conditions, with ESA CCI simulations showing 2 m air temperatures up to 1.5 °C higher on 4 November during the minimum sea-ice period. In contrast, over the Ross Sea the differences in both downwelling longwave radiation and temperature remained small, reaching a maximum of 0.9 °C higher on 31 October (Fig. 11).

These results highlight once again the importance of the boundary sea-ice concentration, with particularly large differences between the higher and lower resolution sea ice datasets over smaller polynyas such as Terra Nova Bay, while the difference is less pronounced over larger polynyas like the Ross Sea, which are already well-resolved in the 25km resolution datasets. Finally, the impact of the polynyas on precipitation in Antarctica was negligible: precipitation amounts in this sector remained very low throughout the period and showed little sensitivity to differences in polynya extent.

https://doi.org/10.5194/egusphere-2025-6183
Preprint. Discussion started: 13 January 2026

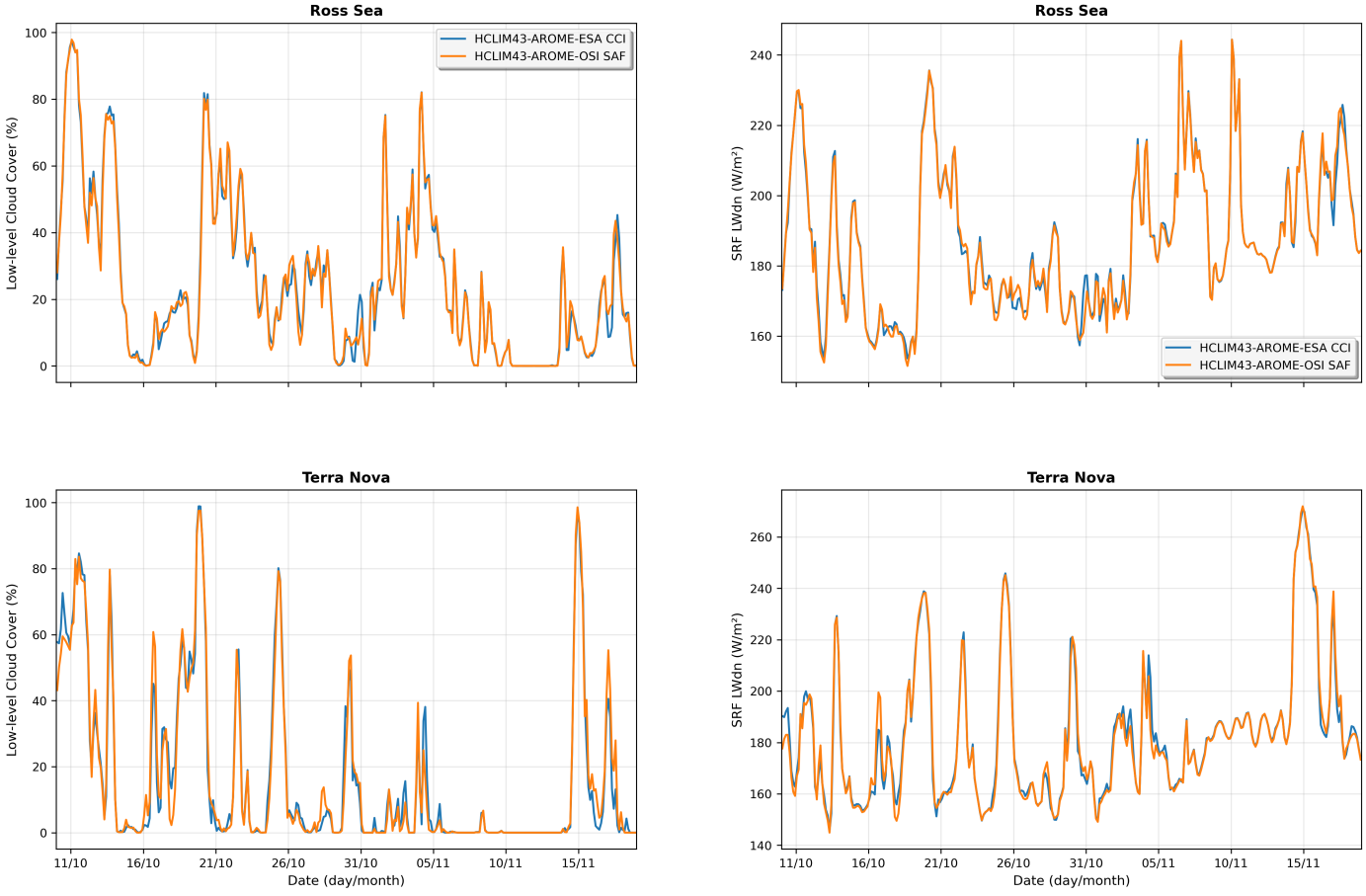

Figure 10. Left panel: Low-level cloud cover (%) from HCLIM simulations forced with ESA CCI and OSI SAF sea-ice concentrations, compared with CARRA reanalysis. Right panel: Downwelling longwave radiation at the surface (W/m^2) from the same simulations and reanalysis. From top to bottom, the panels correspond to the Ross Sea and Terra Nova Bay polynyas.

Figure 12 shows the time series of observed temperature and relative humidity for the Eneide weather station (black line) and the HCLIM simulations using the higher resolution sea-ice concentration boundary condition (orange line) and the coarser sea-ice concentration boundary condition (blue line). The HCLIM simulations clearly follow the time series of the observations but with a consistent cold bias, possibly related to differences in land-sea mask. The three time series showed an increase in temperature and lower values of relative humidity from October 11 to November 13, 2010. For this period, both simulations showed a cold bias of up to 5°C and a positive bias in relative humidity of about 20% (these biases in temperature and relative humidity are common in regional climate models during the katabatic wind events due to the resolution of boundary layer processes, Fonseca et al. (2023)). Interestingly, when the polynya reached its maximum extension, for October 31st, the biases in temperature and RH during the next five days were reduced, especially for temperatures in the simulation using the ESA-CCI boundary condition, reaching a bias of only 2°C with 25% relative humidity. During the rest of the simulation, both experiments

https://doi.org/10.5194/egusphere-2025-6183
Preprint. Discussion started: 13 January 2026

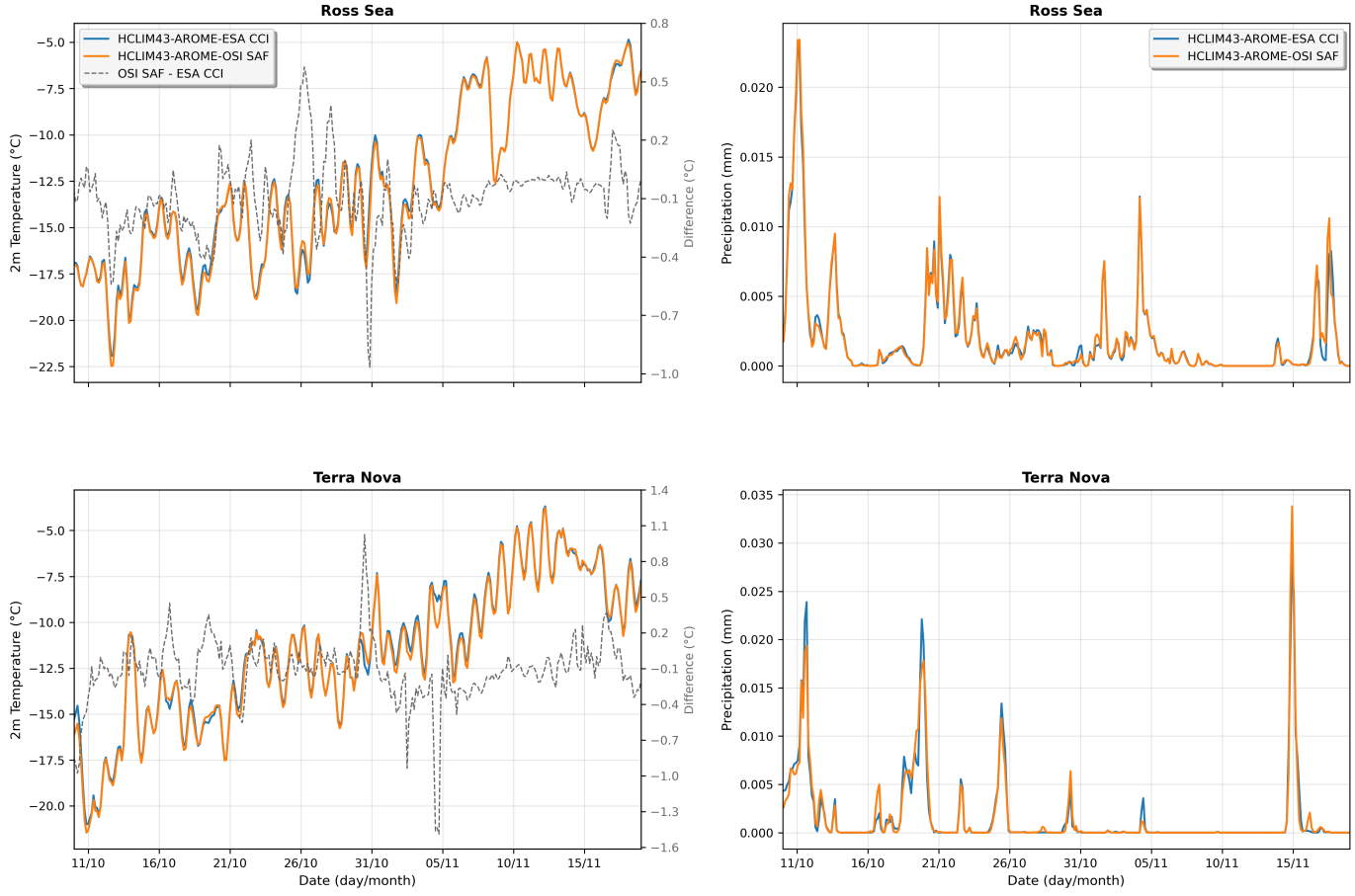

Figure 11. Left panel: 2 m air temperature (°C) from HCLIM simulations forced with ESA CCI and OSI SAF sea-ice concentrations, compared with CARRA reanalysis. Right panel: Precipitation from the same simulations and reanalysis. From top to bottom, the panels correspond to the Ross Sea and Terra Nova Bay polynyas.

were almost identical. Comparing latent heat flux, sensible heat flux and the sea ice area over the Terra Nova polynya (Fig. 7) between both HCLIM experiments, the figure showed a similar flux during almost all of the period, with the exception of a few days before and after the maximum extension of the polynya (minimum sea ice area), where the HCLIM ESA-CCI showed larger latent heat flux up to 35 Wm^{-2}, while HCLIM OSI showed only 30 Wm^{-2}. The opposite occurs for sensible heat flux, with the HCLIM OSI simulating a flux 6 Wm^{-2} larger than HCLIM ESA-CCI. These results show the importance of high resolution sea-ice boundaries in representing extreme events over Antarctica.

https://doi.org/10.5194/egusphere-2025-6183
Preprint. Discussion started: 13 January 2026

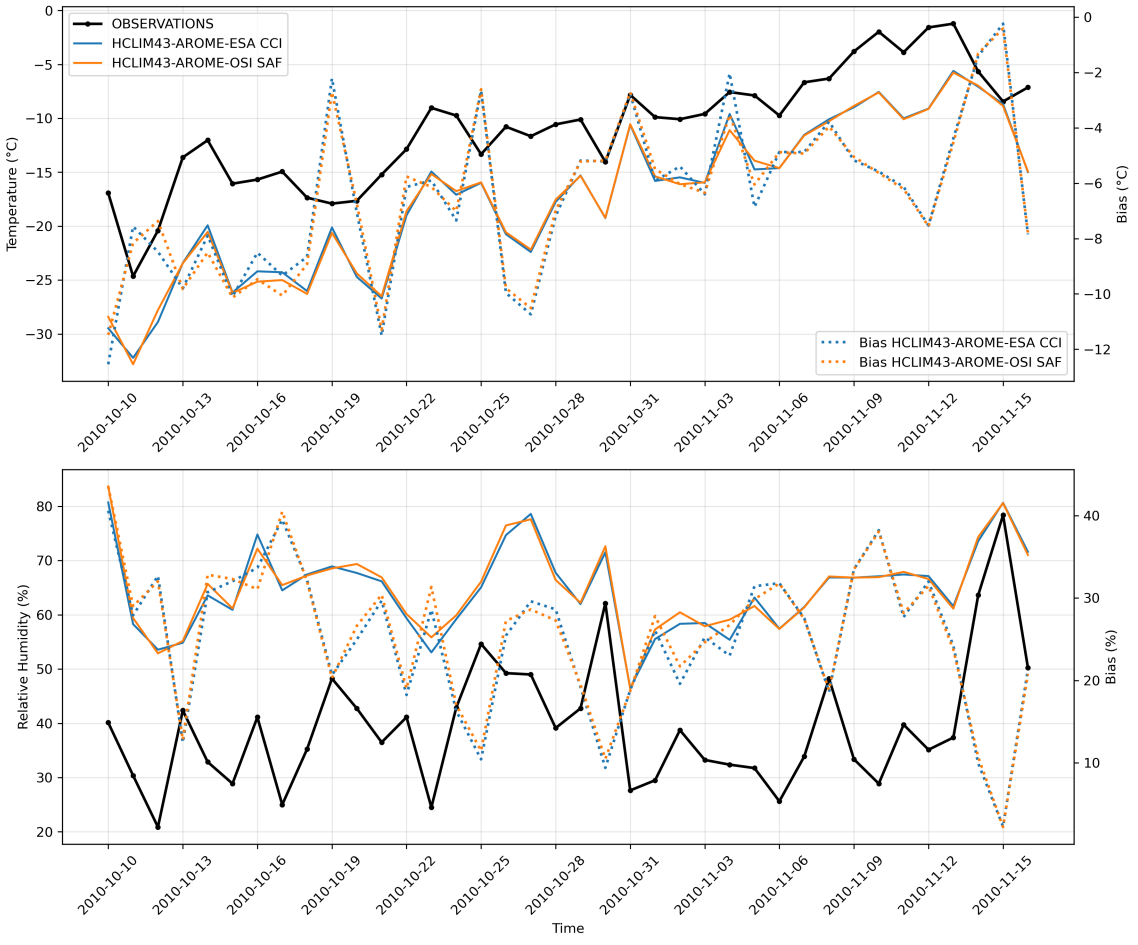

Figure 12. Comparison of observed 2m temperature and 2m relative humidity with HCLIM-AROME for Eneide, Antarctica

5 Discussion and conclusions

In this study we examine the impact of directly using satellite observations of different resolutions of sea-ice concentrations on the representation of polynyas in the HCLIM model, with a focus on the Greenland and Antarctic regions. We assessed the impact of different resolution boundary sea-ice concentrations on sea-ice extent, surface fluxes, clouds, radiation, near-surface temperature and precipitation by comparing simulations forced with ESA CCI and OSI SAF sea-ice products, using CARRA reanalysis as a reference in Greenland. Polynyas play an important role in polar climate processes and representing them accurately, even in relatively high resolution regional climate models has been a long-standing problem. Our simulations at very high resolutions (4km in Greenland and 2.5km in Antarctica) are able to resolve these features and the feedbacks in the atmosphere that result. Our results also demonstrate that the choice of sea-ice boundary conditions directly influences the representation of polynyas in models. In Greenland, discrepancies between the two products were most pronounced in narrow

https://doi.org/10.5194/egusphere-2025-6183
Preprint. Discussion started: 13 January 2026

polynyas such as the Kennedy Channel and the Hall Basin–Robeson Channel, whereas larger features such as the North Water Polynya showed smaller differences. A similar pattern was identified in Antarctica, where the smaller Terra Nova Bay exhibited greater sensitivity than the Ross Sea Polynya. These findings highlight the importance of high-resolution sea-ice products in accurately representing small, dynamic polynyas.

Differences in polynya extent between simulations propagate into the surface–atmosphere exchanges. In both hemispheres the reduced sea ice extent in polynyas coincide with stronger latent heat fluxes, enhancing the local moisture supply and promoting cloud formation. This, in turn, modifies the surface radiation balance through increased downwelling longwave radiation. These effects were most notable in regions where the ESA CCI produced smaller ice concentrations, particularly over the Kennedy Channel, the Hall Basin and Terra Nova Bay. We note however that the underlying atmospheric dynamics are also important sources of humidity that contribute to cloud formation, particularly in our Greenland experiments.

Enhanced cloud cover and longwave radiation resulted in warmer near-surface air temperatures. In Greenland, biases in 2 m air temperature were strongly linked to periods of minimum ice. HCLIM–ESA CCI was found to consistently reduce cold biases in some polynyas more effectively than HCLIM–OSI SAF. The largest warming signal in Antarctica was found in Terra Nova Bay, where differences exceeded 1.5 °C. These results emphasise the sensitivity of surface temperatures to small-scale sea ice variability.

The influence of polynyas on precipitation was limited. In Greenland, the model generally captured precipitation events well, though some were overestimated compared to CARRA. In Antarctica, however, precipitation amounts were very low and largely unaffected by polynya variability. This suggests that their role in local precipitation is secondary compared to latent heat flux and cloud–radiation interactions and vapour transport from lower latitudes.

Our results align with the findings of Semmler et al. (2004); Rinke et al. (2006); Palm et al. (2010); Seo and Yang (2013), which demonstrate the influence of observed sea ice coverage on the polar boundary layer, particularly with regard to surface fluxes and cloud formation. Previous studies (Rinke et al., 2006; Seo and Yang, 2013) show a small near-surface air temperature response to high-resolution boundary sea ice coverage in the boreal summer. These studies employed long (1–15 years) and coarse (25–50 km) RCM simulations over the Arctic. Our short event and high-resolution simulations also confirm these results, except for a few days during the maximum extension of the polynyas. This difference could be explained by the temporal averaging and coarse spatial resolution of the simulations in previous studies. Another difference from Rinke et al. (2006) is that in our simulations, the sea surface temperature is not modified, and our results show the minimum expected impact. In our simulations, the surface modification is derived from the thermodynamic sea ice model (SICE) in HCLIM. This model adjusts the heat diffusion equation and the momentum flux drag according to the presence or absence of sea ice. Future developments implementing a fully coupled ocean-sea ice - atmosphere model will likely improve sea ice concentration during polynya events but our results already demonstrate many of the important processes.

Overall, this study highlights the critical role of sea-ice boundary conditions in regional climate simulations. The results demonstrate that an accurate representation of polynyas is essential for capturing local fluxes, cloud formation and temperature variability, particularly in narrow and coastal polynyas. Further improvements in sea-ice concentration products, particularly

https://doi.org/10.5194/egusphere-2025-6183
Preprint. Discussion started: 13 January 2026

at high resolution, are therefore essential for resolving the coupled atmosphere–ice–ocean system more effectively in polar regions.

Our results furthermore show that an Antarctic reanalysis using a similar set-up to CARRA is plausible and would be improved with the assimilation of high resolution earth observation kind of data, particularly given the relative paucity of in situ observations in Antarctica.

Data availability. Model outputs are available in our Zenodo community at https://zenodo.org/communities/dmi-nckf-hclim-smb.

Sea ice data from the ESA Climate Change Initiative (CCI) are described and can be accessed via the ESA Climate website: https://climate.esa.int/en/projects/sea-ice/. OSI SAF datasets are available from the EUMETSAT website: https://osi-saf.eumetsat.int/products/sea-ice-products.

The following datasets are used in this paper (DOIs link directly to NetCDF files):

- EUMETSAT Ocean and Sea Ice Satellite Application Facility, *Global sea ice concentration climate data record 1978–2020* (v3.1, 2025), OSI-450-a1, doi: 10.15770/EUM_SAF_OSI_0023.
- EUMETSAT Ocean and Sea Ice Satellite Application Facility, *Global sea ice concentration interim climate data record (SSMIS)* (v3.0, 2022), OSI-430-a, doi: 10.15770/EUM_SAF_OSI_0014.
- Lavergne, T., Sørensen, A., Tonboe, R. T., Kreiner, M., Saldo, R., Birkedal, A., Baordo, F., Aspenes, T., and Eastwood, S. (2023): *ESA Sea Ice Climate Change Initiative (Sea_Ice_cci): High(er) Resolution Sea Ice Concentration Climate Data Record Version 3 (SSM/I and SSMIS)*. NERC EDS Centre for Environmental Data Analysis, doi: 10.5285/eade27004395466aaa006135e1b2ad1a.

Author contributions. JATA, RUM, and TL contributed equally to leading this work. JATA led the writing and analysis and was responsible for developing, producing, and post-processing the simulations. RUM contributed substantially to the writing and to conceptualizing the research. TL produced the satellite data and contributed to the writing. RP and OBC contributed to conceptualizing the discussion and supported the production of the simulations.

Competing interests. At least one of the (co-)authors is a member of the editorial board of The Cryosphere.

Acknowledgements. Thanks to the reviewers for their constructive feedback. A big thanks as well to the technical support staff, especially Oskar Landgren, Kristiina Verro, and the HCLIM development team. We also gratefully acknowledge the long term efforts of EUMETSAT OSI SAF and ESA CCI sea ice teams in producing, refining and maintaining immensely valuable sea ice data used directly in this study.

Financial support: R. Mottram's participation in this research was supported by Ocean Cryosphere Exchanges in Antarctica: Impacts on Climate and the Earth system, OCEAN ICE, which is funded by the European Union, Horizon Europe Funding Programme for research and innovation under grant agreement Nr. 101060452, 10.3030/101060452. This is OCEAN ICE contribution number 34.

https://doi.org/10.5194/egusphere-2025-6183
Preprint. Discussion started: 13 January 2026

J.A. Torres-Alvarez and Thomas Lavergne were supported by ESA (through the Climate Change Initiative Sea Ice cci and CCI+ projects, contract no. 4000126449/19/I-NB).

Ole Bøssing Christensen was supported by PolarRES for HCLIM model development. The PolarRES project received funding from the European Union's Horizon 2020 research and innovation programme call H2020-LC-CLA-2018-2019-2020 under grant agreement number 101003590.

https://doi.org/10.5194/egusphere-2025-6183
Preprint. Discussion started: 13 January 2026

References

Batrak, Y., Kourzeneva, E., and Homleid, M.: Implementation of a simple thermodynamic sea ice scheme, SICE version 1.0-38h1, within the ALADIN–HIRLAM numerical weather prediction system version 38h1, Geoscientific Model Development, 11, 3347–3368, https://doi.org/10.5194/gmd-11-3347-2018, 2018.

Batrak, Y., Cheng, B., and Kallio-Myers, V.: Sea ice cover in the Copernicus Arctic Regional Reanalysis, The Cryosphere, 18, 1157–1183, https://doi.org/10.5194/tc-18-1157-2024, 2024.

Belušić, D., de Vries, H., Dobler, A., Landgren, O., Lind, P., Lindstedt, D., Pedersen, R. A., Sánchez-Perrino, J. C., Toivonen, E., van Ulft, B., Wang, F., Andrae, U., Batrak, Y., Kjellström, E., Lenderink, G., Nikulin, G., Pietikäinen, J.-P., Rodríguez-Camino, E., Samuelsson, P., van Meijgaard, E., and Wu, M.: HCLIM38: a flexible regional climate model applicable for different climate zones from coarse to convection-permitting scales, Geoscientific Model Development, 13, 1311–1333, https://doi.org/10.5194/gmd-13-1311-2020, 2020.

Bengtsson, L., Andrae, U., Aspelien, T., Batrak, Y., Calvo, J., de Rooy, W., Gleeson, E., Hansen-Sass, B., Homleid, M., Hortal, M., Ivarsson, K.-I., Lenderink, G., Niemelä, S., Nielsen, K. P., Onvlee, J., Rontu, L., Samuelsson, P., Muñoz, D. S., Subias, A., Tijm, S., Toll, V., Yang, X., and Køltzow, M. : The HARMONIE–AROME Model Configuration in the ALADIN–HIRLAM NWP System, Monthly Weather Review, 145, 1919–1935, https://doi.org/10.1175/MWR-D-16-0417.1, 2017.

Berg, P., Döscher, R., and Koenigk, T.: Impacts of using spectral nudging on regional climate model RCA4 simulations of the Arctic, Geoscientific Model Development, 6, 849–859, https://doi.org/10.5194/gmd-6-849-2013, 2013.

Blanchard-Wrigglesworth, E., Bitz, C. M., and Holland, M. M.: Influence of initial conditions and climate forcing on predicting Arctic sea ice: ARCTIC SEA ICE PREDICTABILITY, Geophysical Research Letters, 38, n/a–n/a, https://doi.org/10.1029/2011GL048807, 2011.

Day, J. J., Hawkins, E., and Tietsche, S.: Will Arctic sea ice thickness initialization improve seasonal forecast skill?, Geophysical Research Letters, 41, 7566–7575, https://doi.org/10.1002/2014GL061694, 2014.

Fettweis, X., Hofer, S., Krebs-Kanzow, U., Amory, C., Aoki, T., Berends, C. J., Born, A., Box, J. E., Delhasse, A., Fujita, K., Gierz, P., Goelzer, H., Hanna, E., Hashimoto, A., Huybrechts, P., Kapsch, M.-L., King, M. D., Kittel, C., Lang, C., Langen, P. L., Lenaerts, J. T. M., Liston, G. E., Lohmann, G., Mernild, S. H., Mikolajewicz, U., Modali, K., Mottram, R. H., Niwano, M., Noël, B., Ryan, J. C., Smith, A., Streffing, J., Tedesco, M., van de Berg, W. J., van den Broeke, M., van de Wal, R. S. W., van Kampenhout, L., Wilton, D., Wouters, B., Ziemen, F., and Zolles, T.: GrSMBMIP: intercomparison of the modelled 1980–2012 surface mass balance over the Greenland Ice Sheet, The Cryosphere, 14, 3935–3958, https://doi.org/10.5194/tc-14-3935-2020, 2020.

Fonseca, R., Francis, D., Aulicino, G., Mattingly, K. S., Fusco, G., and Budillon, G.: Atmospheric controls on the Terra Nova Bay polynya occurrence in Antarctica, Climate Dynamics, 61, 5147–5169, https://doi.org/10.1007/s00382-023-06845-0, 2023.

Golledge, N. R., Keller, E. D., Gossart, A., Malyarenko, A., Bahamondes-Dominguez, A., Krapp, M., Jendersie, S., Lowry, D. P., Alevropoulos-Borrill, A., and Notz, D.: Antarctic coastal polynyas in the global climate system, Nature Reviews Earth & Environment, 6, 126–139, https://doi.org/10.1038/s43017-024-00634-x, 2025.

Kern, S., Lavergne, T., Notz, D., Pedersen, L. T., Tonboe, R. T., Saldo, R., and Sørensen, A. M.: Satellite passive microwave sea-ice concentration data set intercomparison: closed ice and ship-based observations, The Cryosphere, 13, 3261–3307, https://doi.org/10.5194/tc-13-3261-2019, 2019.

Kern, S., Lavergne, T., Notz, D., Pedersen, L. T., and Tonboe, R.: Satellite passive microwave sea-ice concentration data set inter-comparison for Arctic summer conditions, The Cryosphere, 14, 2469–2493, https://doi.org/10.5194/tc-14-2469-2020, 2020.

https://doi.org/10.5194/egusphere-2025-6183
Preprint. Discussion started: 13 January 2026

Kern, S., Lavergne, T., Pedersen, L. T., Tonboe, R. T., Bell, L., Meyer, M., and Zeigermann, L.: Satellite passive microwave sea-ice concentration data set intercomparison using Landsat data, The Cryosphere, 16, 349–378, https://doi.org/10.5194/tc-16-349-2022, 2022.

Koenigk, T., Berg, P., and Döscher, R.: Arctic climate change in an ensemble of regional CORDEX simulations, Polar Research, https://doi.org/10.3402/polar.v34.24603, 2015.

Kwok, R. and Rothrock, D. A.: Decline in Arctic sea ice thickness from submarine and ICESat records: 1958-2008: ARCTIC SEA ICE THICKNESS, Geophysical Research Letters, 36, n/a–n/a, https://doi.org/10.1029/2009GL039035, 2009.

Lavergne, T., Sørensen, A. M., Kern, S., Tonboe, R., Notz, D., Aaboe, S., Bell, L., Dybkjær, G., Eastwood, S., Gabarro, C., Heygster, G., Killie, M. A., Brandt Kreiner, M., Lavelle, J., Saldo, R., Sandven, S., and Pedersen, L. T.: Version 2 of the EUMETSAT OSI SAF and ESA CCI sea-ice concentration climate data records, The Cryosphere, 13, 49–78, https://doi.org/10.5194/tc-13-49-2019, 2019.

Lavergne, T., Sørensen, A., Tonboe, R., Strong, C., Kreiner, M., Saldo, R., Birkedal, A., Baordo, F., Rusin, J., Aspenes, T., and Eastwood, S.: Monitoring of Sea Ice Concentration, Area, and Extent in the polar regions : 40+ years of data from EUMETSAT OSI SAF and ESA CCI, https://doi.org/10.5281/zenodo.10014535, 2023a.

Lavergne, T., Sørensen, A., Tonboe, R. T., Kreiner, M., Saldo, R., Birkedal, A., Baordo, F., Aspenes, T., and Eastwood, S.: ESA Sea Ice Climate Change Initiative (Sea_Ice_cci): High(er) Resolution Sea Ice Concentration Climate Data Record Version 3 (SSM/I and SSMIS), https://doi.org/10.5285/EADE27004395466AAA006135E1B2AD1A, 2023b.

Lee, Y. J., Maslowski, W., Cassano, J. J., Clement Kinney, J., Craig, A. P., Kamal, S., Osinski, R., Seefeldt, M. W., Stroeve, J., and Wang, H.: Causes and evolution of winter polynyas north of Greenland, The Cryosphere, 17, 233–253, https://doi.org/10.5194/tc-17-233-2023, 2023.

Lenderink, G. and Holtslag, A. A. M.: An updated length-scale formulation for turbulent mixing in clear and cloudy boundary layers, Quarterly Journal of the Royal Meteorological Society, 130, 3405–3427, https://doi.org/https://doi.org/10.1256/qj.03.117, 2004.

Lind, P., Belušić, D., Médus, E., Dobler, A., Pedersen, R. A., Wang, F., Matte, D., Kjellström, E., Landgren, O., Lindstedt, D., Christensen, O. B., and Christensen, J. H.: Climate change information over Fenno-Scandinavia produced with a convection-permitting climate model, Climate Dynamics, https://doi.org/10.1007/s00382-022-06589-3, 2022.

Lo, J. C.-F., Yang, Z.-L., and Pielke Sr., R. A.: Assessment of three dynamical climate downscaling methods using the Weather Research and Forecasting (WRF) model, Journal of Geophysical Research: Atmospheres, 113, https://doi.org/https://doi.org/10.1029/2007JD009216, 2008.

Ludwig, V., Spreen, G., Haas, C., Istomina, L., Kauker, F., and Murashkin, D.: The 2018 North Greenland polynya observed by a newly introduced merged optical and passive microwave sea-ice concentration dataset, The Cryosphere, 13, 2051–2073, https://doi.org/10.5194/tc-13-2051-2019, 2019.

Moore, G. W. K., Schweiger, A., Zhang, J., and Steele, M.: What Caused the Remarkable February 2018 North Greenland Polynya?, Geophysical Research Letters, 45, https://doi.org/10.1029/2018GL080902, 2018.

Moore, G. W. K., Howell, S. E. L., and Brady, M.: Evolving relationship of Nares Strait ice arches on sea ice along the Strait and the North Water, the Arctic's most productive polynya, Scientific Reports, 13, 9809, https://doi.org/10.1038/s41598-023-36179-0, 2023.

Morales Maqueda, M. A., Willmott, A. J., and Biggs, N. R. T.: Polynya Dynamics: a Review of Observations and Modeling, Reviews of Geophysics, 42, https://doi.org/https://doi.org/10.1029/2002RG000116, 2004.

Mottram, R., Hansen, N., Kittel, C., van Wessem, J. M., Agosta, C., Amory, C., Boberg, F., van de Berg, W. J., Fettweis, X., Gossart, A., van Lipzig, N. P. M., van Meijgaard, E., Orr, A., Phillips, T., Webster, S., Simonsen, S. B., and Souverijns, N.: What is the surface mass balance

https://doi.org/10.5194/egusphere-2025-6183
Preprint. Discussion started: 13 January 2026

of Antarctica? An intercomparison of regional climate model estimates, The Cryosphere, 15, 3751–3784, https://doi.org/10.5194/tc-15-3751-2021, 2021.

Mottram, R. H. and Consortium, P.: High Resolution Polar Regional Climate Modelling: Experimental Protocol for a community approach, Geoscientific Model Development.

Noel, M., Masson, S., and Rousset, C.: Atmospheric Response to Antarctic Coastal Polynyas, Journal of Geophysical Research: Atmospheres, 130, e2025JD043 319, https://doi.org/https://doi.org/10.1029/2025JD043319, 2025.

Notz, D. and Community, S.: Arctic Sea Ice in CMIP6, Geophysical Research Letters, 47, e2019GL086 749, https://doi.org/https://doi.org/10.1029/2019GL086749, 2020.

OSI SAF and EUMETSAT SAF On Ocean And Sea Ice: Global Sea Ice Concentration Climate Data Record v3.0 - Multimission, https://doi.org/10.15770/EUM_SAF_OSI_0013, 2022.

Palm, S. P., Strey, S. T., Spinhirne, J., and Markus, T.: Influence of Arctic sea ice extent on polar cloud fraction and vertical structure and implications for regional climate, Journal of Geophysical Research: Atmospheres, 115, https://doi.org/https://doi.org/10.1029/2010JD013900, 2010.

Radu, R., Déqué, M., and Somot, S.: Spectral nudging in a spectral regional climate model, Tellus A, 60, 898–910, https://doi.org/https://doi.org/10.1111/j.1600-0870.2008.00341.x, 2008.

Rinke, A., Maslowski, W., Dethloff, K., and Clement, J.: Influence of sea ice on the atmosphere: A study with an Arctic atmospheric regional climate model, Journal of Geophysical Research: Atmospheres, 111, https://doi.org/https://doi.org/10.1029/2005JD006957, 2006.

Roach, L. A., Dörr, J., Holmes, C. R., Massonnet, F., Blockley, E. W., Notz, D., Rackow, T., Raphael, M. N., O'Farrell, S. P., Bailey, D. A., and Bitz, C. M.: Antarctic Sea Ice Area in CMIP6, Geophysical Research Letters, 47, e2019GL086 729, https://doi.org/10.1029/2019GL086729, _eprint: https://agupubs.onlinelibrary.wiley.com/doi/pdf/10.1029/2019GL086729, 2020.

Rooy, W. C. d. and Siebesma, A. P.: A Simple Parameterization for Detrainment in Shallow Cumulus, Monthly Weather Review, 136, 560 – 576, https://doi.org/10.1175/2007MWR2201.1, 2008.

Sauerland, F., Huot, P.-V., Marchi, S., Fichefet, T., Goosse, H., Haubner, K., Klein, F., Massonnet, F., Mezzina, B., Moreno-Chamarro, E., Ortega, P., Pattyn, F., Pelletier, C., Verfaillie, D., Zipf, L., and van Lipzig, N.: EC-Earth- and ERA5-driven ensemble hindcasts with the fully coupled ice-sheet–ocean–sea ice–atmosphere–land circum-Antarctic model PARASO, EGUsphere, pp. 1–30, https://doi.org/10.5194/egusphere-2025-2889, 2025.

Schyberg, H., Yang, X., Køltzow, M. A. , Amstrup, B., Bakketun, , Bazile, E., Bojarova, J., Box, J. E., Dahlgren, P., Hagelin, S., Homleid, M., Horányi, A., Høyer, J., Johansson, , Killie, M. A., Körnich, H., Le Moigne, P., Lindskog, M., Manninen, T., Nielsen Englyst, P., Nielsen, K. P., Olsson, E., Palmason, B., Peralta Aros, C., Randriamampianina, R., Samuelsson, P., Stappers, R., Støylen, E., Thorsteinsson, S., Valkonen, T., and Wang, Z. Q.: Arctic regional reanalysis on single levels from 1991 to present, https://doi.org/10.24381/cds.713858f6, published: Copernicus Climate Change Service (C3S) Climate Data Store (CDS), 2020.

Semmler, T., Jacob, D., Schlünzen, K. H., and Podzun, R.: Influence of Sea Ice Treatment in a Regional Climate Model on Boundary Layer Values in the Fram Strait Region, Monthly Weather Review, 132, 985 – 999, https://doi.org/10.1175/1520-0493(2004)132<0985:IOSITI>2.0.CO;2, 2004.

Seo, H. and Yang, J.: Dynamical response of the Arctic atmospheric boundary layer process to uncertainties in sea-ice concentration, Journal of Geophysical Research: Atmospheres, 118, 12,383–12,402, https://doi.org/https://doi.org/10.1002/2013JD020312, 2013.

Stroeve, J. C., Kattsov, V., Barrett, A., Serreze, M., Pavlova, T., Holland, M., and Meier, W. N.: Trends in Arctic sea ice extent from CMIP5, CMIP3 and observations, Geophysical Research Letters, 39, 2012GL052 676, https://doi.org/10.1029/2012GL052676, 2012.

https://doi.org/10.5194/egusphere-2025-6183
Preprint. Discussion started: 13 January 2026

Thompson, L., Smith, M., Thomson, J., Stammerjohn, S., Ackley, S., and Loose, B.: Frazil ice growth and production during katabatic wind events in the Ross Sea, Antarctica, The Cryosphere, 14, 3329–3347, https://doi.org/10.5194/tc-14-3329-2020, 2020.

Tietsche, S., Notz, D., Jungclaus, J. H., and Marotzke, J.: Assimilation of sea-ice concentration in a global climate model – physical and statistical aspects, Ocean Science, 9, 19–36, https://doi.org/10.5194/os-9-19-2013, 2013.

Vincent, R. F.: A Study of the North Water Polynya Ice Arch using Four Decades of Satellite Data, Scientific Reports, 9, 20 278, https://doi.org/10.1038/s41598-019-56780-6, 2019.

Von Storch, H., Langenberg, H., and Feser, F.: A Spectral Nudging Technique for Dynamical Downscaling Purposes, Monthly Weather Review, 128, 3664–3673, https://doi.org/10.1175/1520-0493(2000)128<3664:ASNTFD>2.0.CO;2, 2000.

Wei, Z., Zhang, Z., Vihma, T., Wang, X., and Chen, Y.: An overview of Antarctic polynyas: sea ice production, forcing mechanisms, temporal variability and water mass formation, Advances in Polar Science, 32, 295–311, https://doi.org/10.13679/j.advps.2021.0026, 2021.